



Development and Application of Rock Fracture Propagation Numerical Simulation System

Hui Wang · Hang Zhou · Shichang Shang · Cheng Jiang

Received: 28 June 2021 / Accepted: 30 January 2022 / Published online: 18 February 2022
© The Author(s), under exclusive licence to Springer Nature Switzerland AG 2022

Abstract The mechanism of rock fracture evolution under loading has always been the focus of rock mechanics community. In this paper, to realize the development of rock crack propagation simulation system based on ABAQUS platform, the failure criteria which involve maximum tensile stress criterion, the maximum compressive stress criterion and the Mohr–Coulomb failure criterion (M–C) are programmed into the VUMAT subroutine, and the failure element deletion algorithm is introduced to investigate the deformation and failure process of rock blocks under load. Then, the proposed system is used to analyze the progressive failure process of rock samples under loading. By comparing with the test results, the causes and characteristics of crack expansion are studied, meanwhile the different forms of the rock failure process are explored.

Keywords The mechanism of rock fracture evolution · The failure criteria · Failure element deletion algorithm · The development of simulation system

1 Introduction

Fracture is a small fracture structure with no significant displacement of the rock blocks on both sides of rock mass after bearing stress fracture, which is a universal geological structure. In practical engineering, defects such as cracks in rocks are unavoidable engineering phenomena, whose unstable development will cause instability of rock mass engineering. Therefore, the research on the mechanics mechanism of rock fracture propagation has attracted more and more attention from the academic and engineering circles (Wang 2009).

There are many forms and methods for the research on fracture and crack propagation of rock materials. In the model test research, Miao et al. (2018) studied the crack evolution process of sandstone samples with different defect inclination angles under uniaxial compression test. Li (2005) based on the real-time CT scanning test results during loading, the crack propagation law is analyzed. Sun et al. (2020) proposed a method of combining acoustic emission testing with infrared spectrum characteristics to analyze the stability of hard rock pillars (HRP) sandwiched between extremely steep and thick coal seams. In order to

H. Wang (✉) · H. Zhou · S. Shang
College of Resources, Shandong University
of Science and Technology, Tai'an, Shandong 271019,
The People's Republic of China
e-mail: wanghui2004315@163.com

H. Wang
College of Civil Engineering and Architecture, Shandong
University of Science and Technology, Qingdao 266590,
Shandong, The People's Republic of China

C. Jiang
Lianyungang Architectural Design and Research
Institute Co., Ltd, Lianyungang 222000, Jiangsu,
The People's Republic of China

obtain the crack growth characteristics of rocks under post-peak cyclic loading, Tang et al. (2020) adopted the three-point bending test method combined with digital image correlation (DIC) and acoustic emission (AE) technology to test the granite notched-beam. Yu et al. (2021) conducted a series of triaxial compression tests on sandstone coal (SC) and sandstone coal bolt (SCB) at different angles, and evaluated the fracture process of the sample by establishing crack initiation stress index (CI) and crack damage stress index (CD). Wu et al. (2020a, b) conducted a series of uniaxial compression tests on inclined rock coal (RC) composite specimens. The results show that the failure of RC composite specimens is caused by tensile and shear cracks.

The model test can well obtain the law of fracture expansion, but the model test takes long time and costs high (Sanchez et al. 2020). Moreover, fracture propagation of specimens is extremely complex. After fracture initiation, the fracture no longer maintains a plane and forms a distorted plane, which is difficult to analyze. The development of computer technology has greatly aided the work of numerical simulation. The numerical simulation method is widely used to analyze the fracture propagation in rocks. Discrete element method-DEM (Matsuda and Iwase 2002; Yang et al. 2020; Gui et al. 2016; Aliabadian et al. 2014) treats jointed rock mass as consisting of discrete rock blocks and jointed surfaces between them, allowing the blocks to translate, rotate and deform, while the jointed surface can be compressed, separated or slid. In order to better reflect the impact of discontinuities such as fractures and their extensions on the mechanical behavior of rock mass, displacement discontinuity method -DDM (Li et al. 2014, 2012; Marji 2015) has been applied by scholars to study the problem of elastomers with discontinuities. The principle of finite element method—FEM is to discrete the continuous solution domain into a combination of a group of elements, and use the assumed approximate function in each element to slice to represent the unknown field function to be solved in the solution domain. The approximate function is usually expressed by the numerical interpolation function of the unknown field function and its derivative at each node of the element. Thus, a continuous infinite degree of freedom problem becomes a discrete finite degree of freedom problem. However, the crack tip mesh of the finite element

method model needs to be segmented very fine, and each crack expansion step needs to be segmented once, which increases the complexity of the simulation process. XFEM (Wang et al. 2017, 2020a, b, c; Sheng et al. 2018; Feng and Gray 2019) can effectively solve the above problems. Multiple studies coupled finite element-discrete element (Wu et al. 2019; Trivino and Mohanty 2015; Wu et al. 2020a, b) to explore the interaction between continuous media and discrete media have broadened the application field of numerical simulation methods. Other methods include embedded discrete Fracture model—EDFM (Trippopoom et al. 2019; Huang et al. 2019; Wang et al. 2019), etc.

In the model, Qian et al. (2020) applied stress waves to numerical simulation specimens with three-dimensional surface defects until failure, and analyzed the influence of different crack angles on the initiation and propagation of wing cracks, anti-wing cracks and shell cracks under dynamic loading conditions. Silva and Ranjith (2020) used discrete element program PFC3D-5.0 to simulate the influence of rock joints on the fracture behavior of SCDA (SCDA is a cementitious compound), and further studied the law of crack growth. Ofoegbu and Smart (2019) developed a simulation method for the initiation, deformation and propagation of discrete fractures in rock continuum analysis, and provided numerical simulation to evaluate the performance of this method for analytical solutions and laboratory data. Sanchez et al. (2020) proposed a numerical method to study the interaction between hydraulic fractures and natural fractures by using finite element method and predict the fracture expansion direction. Tang and Li (2015) used particle flow software PFC to simulate the crack propagation process and characteristics of preset single fractured rock under bidirectional compression. Chen et al. (2020) developed a quasi-continuous model to describe fracture propagation in fractured rocks. The model can satisfactorily simulate fracture propagation in tension, shear and mixed modes.

However, the above work is only applicable to the sample simulation in specific cases. In fact, under complex stress conditions, the rock may undergo compression, tension or shear failure. Therefore, it is necessary to propose a new rock fracture propagation simulation system to meet all cases. The system is of great significance to reveal the internal relationship between the whole process of micro fracture

development and macro fracture development under uniaxial compression.

2 Numerical Simulation of Rock Failure Process Under Load

ABAQUS is a powerful and versatile set of finite element software for engineering simulation that solves problems ranging from relatively simple linear analysis to many complex nonlinear problems. ABAQUS can simulate many problems in the field of engineering, such as heat conduction (Xia et al. 2020), thermoelectric coupling analysis (Li 2012) and geotechnical mechanics analysis (Wang et al. 2020a, b, c).

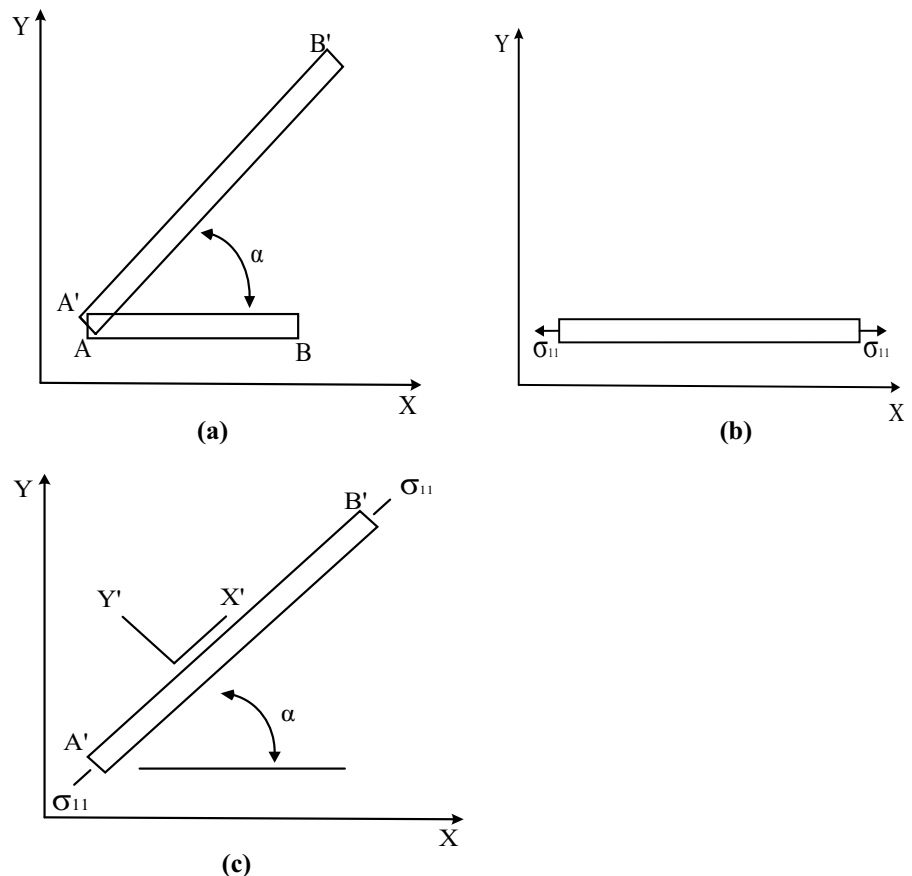
The element deletion function is a method to overcome the defects of the finite element itself, which is based on continuum mechanics. In continuum physics, the object to be studied needs to be continuous, that is, the material domain is continuous in space. In such a theoretical framework, the element will not

disappear. However, in the actual situation, due to the existence of damage and fracture, some elements are bound to disappear or completely fail. Therefore, in order to simulate this situation, the ABAQUS platform provides element failure function.

In user subroutine VUMAT, all strain measures are calculated with respect to the mid increment configuration. All tensor quantities are defined in the co-rotational coordinate system that rotates with the material point. To illustrate what this means in terms of stresses, consider the bar shown in Fig. 1a, which is stretched and rotated from its original configuration, AB, to its new position, A'B'. This deformation can be obtained in two stages; the bar is first stretched, as shown in Fig. 1b, and is then rotated by applying a rigid body rotation to it, as shown in Fig. 1c.

The stress in the bar after it has been stretched is σ_{11} , and this stress does not change during the rigid body rotation. The X'Y' coordinate system that rotates as a result of the rigid body rotation is the co-rotational coordinate system. The stress tensor and

Fig. 1 a Stretched and rotated bar; b Stretching of bar; c Rigid body rotation of bar



state variables are, therefore, computed directly and updated in user subroutine VUMAT using the strain tensor since all of these quantities are in the co-rotational system.

In order to verify the validity of the simulation system for rock fracture expansion, this section adopts the maximum tensile stress criterion, maximum compressive stress criterion and Mohr–Coulomb criterion respectively to analyze the failure process of rock sample.

The mechanical parameters involved in the numerical simulation are selected from the rock mass mechanical parameters of coal and rock matrix materials tested by Sun et al. (2014) (Table 1).

2.1 Numerical Simulation of Rock Failure Process Based on Maximum Tensile Stress Criterion

The maximum tensile stress criterion of the element (Sun et al. 2014):

$$f = |\sigma_1| - \sigma_t = 0 \quad (1)$$

where, σ_1 is the first principal stress of the element ($\sigma_1 \geq \sigma_2 \geq \sigma_3$, the tensile stress is positive and the compressive stress is negative); σ_t is the static tensile strength of the matrix. The ultimate tensile strength of complete coal and rock under triaxial stress is taken and determined by triaxial experiment. In order to better simulate the stress concentration phenomenon during the failure process of the sample, the calculation model is selected as shown in Fig. 2.

For this model, normal constraints are imposed at the bottom of the model, displacement-controlled loading is adopted for compression on the upper surface, the maximum displacement of loading is 15 mm, and the loading rate is controlled as 0.005 mm/step. In ABAQUS software platform, the dynamic analysis step is adopted, the shape of the model unit is quadrilateral, and the Structured partitioning method is adopted. The plane strain problem is adopted in the calculation

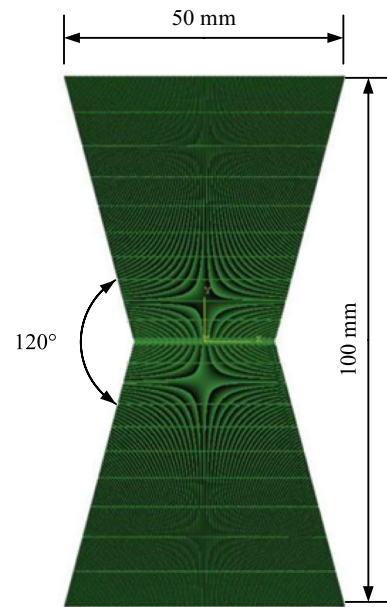


Fig. 2 Calculation model

model, and the model is isotropic within the calculation range (Fig. 3).

Under the vertical tensile of the model, stress concentration occurs at the crack tip at first. With the increase of loading, the element near the stress concentration area meets the failure conditions and cracks initiate. After that, the initial crack extends to the interior element penetrates the whole model.

2.2 Numerical Simulation of Rock Failure Process Based on Maximum Compressive Stress Criterion

The maximum compressive stress criterion of the element (Sun et al. 2014):

$$f = |\sigma_3| - \sigma_c = 0 \quad (2)$$

Table 1 Rock mass mechanical parameters of rock materials used in the model

Material	Elastic modulus (GPa)	Poisson's ratio	Cohesion (MPa)	The angle of internal friction	Compressive strength (MPa)	Tensile strength (MPa)
Coal and rock matrix	2.93	0.38	3.11	40.90	33.30	4.00

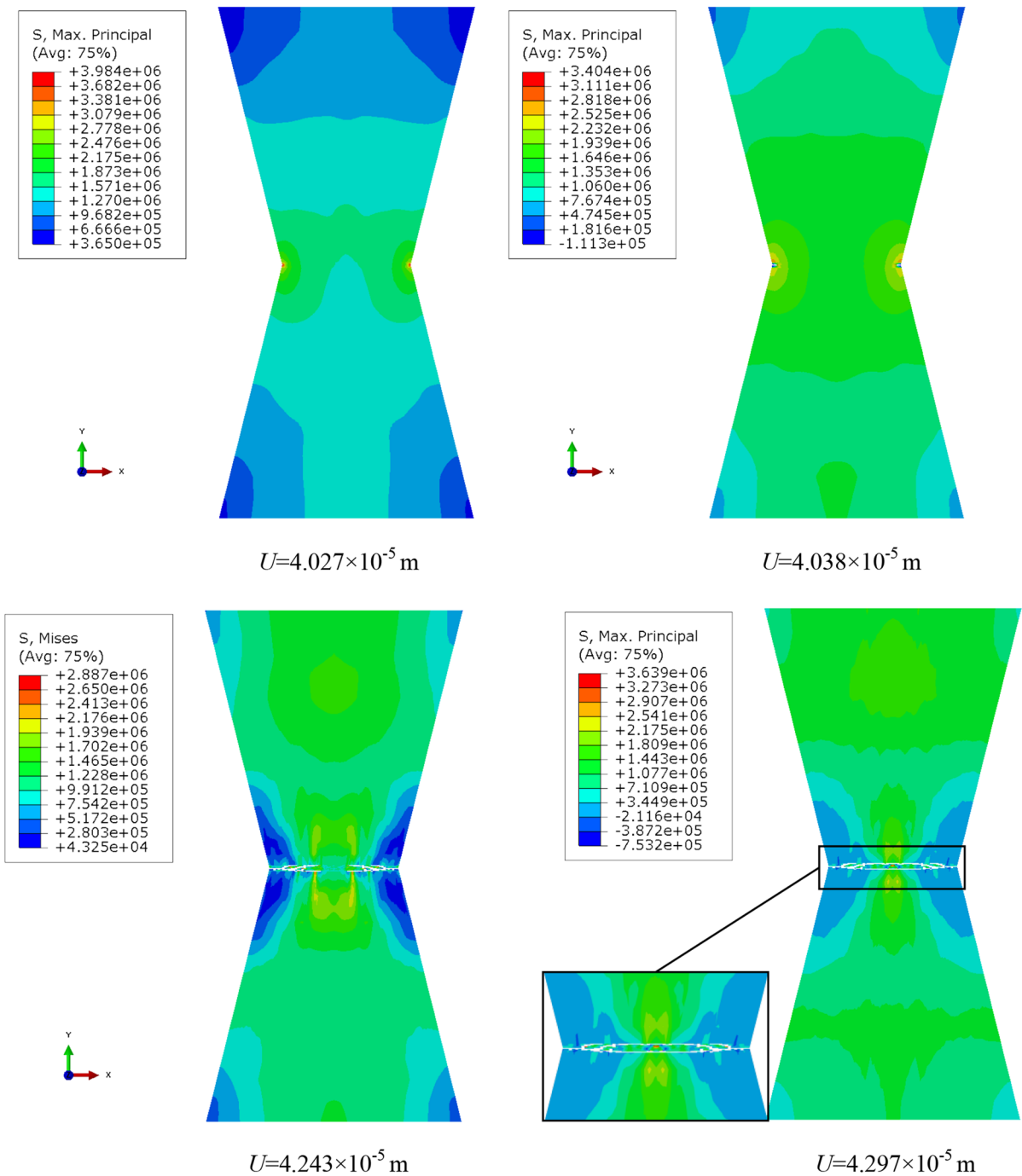


Fig. 3 Dynamic process of model failure under tension (Stress unit unit: Pa)

Among them, σ_3 is the third principal stress of the element ($\sigma_1 \geq \sigma_2 \geq \sigma_3$, tensile stress is positive, and compressive stress is negative). σ_c is the static compressive strength of the matrix. Considering the

influence of multiaxial stress, σ_c is the ultimate compressive strength of the complete rock under triaxial stress, which is determined by triaxial experiments.

The calculation model is shown in Fig. 2, and the calculation parameters are shown in Table 1.

The numerical simulation of rock failure process based on minimum compressive stress criterion is similar to the numerical simulation of rock failure process based on maximum principal stress criterion. The maximum displacement of loading is 15 mm, and the loading rate is controlled as 0.005 mm/step.

Under the action of vertical compression state, stress concentration phenomenon appears in the model. With the increase of loading, the element near the stress concentration area conforms to the failure conditions and cracks start, and then the initial crack extends to the interior until the model is destroyed (Fig. 4).

2.3 Numerical Simulation of Rock Failure Process Based on M–C Criterion

The biggest advantage of the M–C criterion is that it reflects the S–D effect of different compressive strengths of rock and soil materials and the sensitivity to normal stress, which is simple and practical. Material parameters are determined by various conventional experimental instruments and methods. Therefore, the M–C criterion is widely used in rock and soil mechanics and plastic theory.

The M–C criterion for matrix element failure can be expressed as (Sun et al. 2014):

$$f = (\sigma_1 - \sigma_3) - (\sigma_1 + \sigma_3) \sin \phi - 2c \cdot \cos \phi = 0 \quad (3)$$

σ_1 , σ_2 , σ_3 represent the first principal stress, the second principal stress, and the third principal stress. c , ϕ are the yield or failure parameters of the material, namely the cohesive force and internal friction angle of the material.

The principal stress is the normal stress when the shear stress on a micro area element with $n = (n_1, n_2, n_3)$ is zero at a certain point in the object. In this case, direction of the n is called the principal direction of the stress at this point. The normal stress of a point on a micro area element takes a standing value in the principal direction of the stress when the normal vector n of the area changes. For the stress tensor $\sigma_{ij}(i, j = 1, 2, 3)$ at a point, there are generally three principal stresses. When they satisfy the cubic Eq. (4), the solution to the cubic equation is the

principal stress $\sigma_i(i = 1, 2, 3)$. For the stress tensor at a given point, the principal stress is the invariant under coordinate transformation.

$$\sigma_i^3 - I_1 \sigma_i^2 - I_2 \sigma_i - I_3 = 0 \quad (4)$$

I_1 is the first invariant of the stress tensor, I_2 is the second invariant of the stress tensor, and I_3 is the third invariant of the stress tensor.

The overall size of this model (Fig. 5 for the calculation model) is $W \times L = 50 \text{ mm} \times 100 \text{ mm}$. The fracture is located in the center of the model and perpendicular to the rock mass surface. The angle between the fracture and the horizontal line is 45° , and the fracture length is 20 mm. The bottom of the model is fixed, and the upper surface is compressed by displacement control loading. The maximum displacement of loading is 15 mm, and the loading rate is controlled as 0.005 mm/step. The calculation parameters are shown in Table 1.

First of all, stress concentration appears at the crack tip. With the increase of deformation and loading stress, the element near the stress concentration area meets the failure condition of M–C criterion and cracks occur. After that, the number of element damage increases and the model is destroyed (Fig. 6).

The above simulation results reveal that the stress state around the microcrack tip is very complex and there is obvious stress concentration (Li et al. 2015). During the compression process of the specimen, the stress intensity of rock element near the crack tip increases continuously until it exceeds the rock mass strength, leading to the failure of rock element. Finally, the rock damage element increases until the whole rock specimen is seriously damaged.

2.4 Development and Application of Rock Fracture Propagation Simulation System

Under complex stress conditions, the rock may undergo compression, tension or shear failure. The innovation of this system is to take the maximum compressive stress, maximum tensile stress and M–C criterion as the failure criterion of matrix element under complex stress. The failure of element is determined by the first stress state and failure criterion of any element.

Under the action of load, when the stress state of a certain element in the model meets any of the

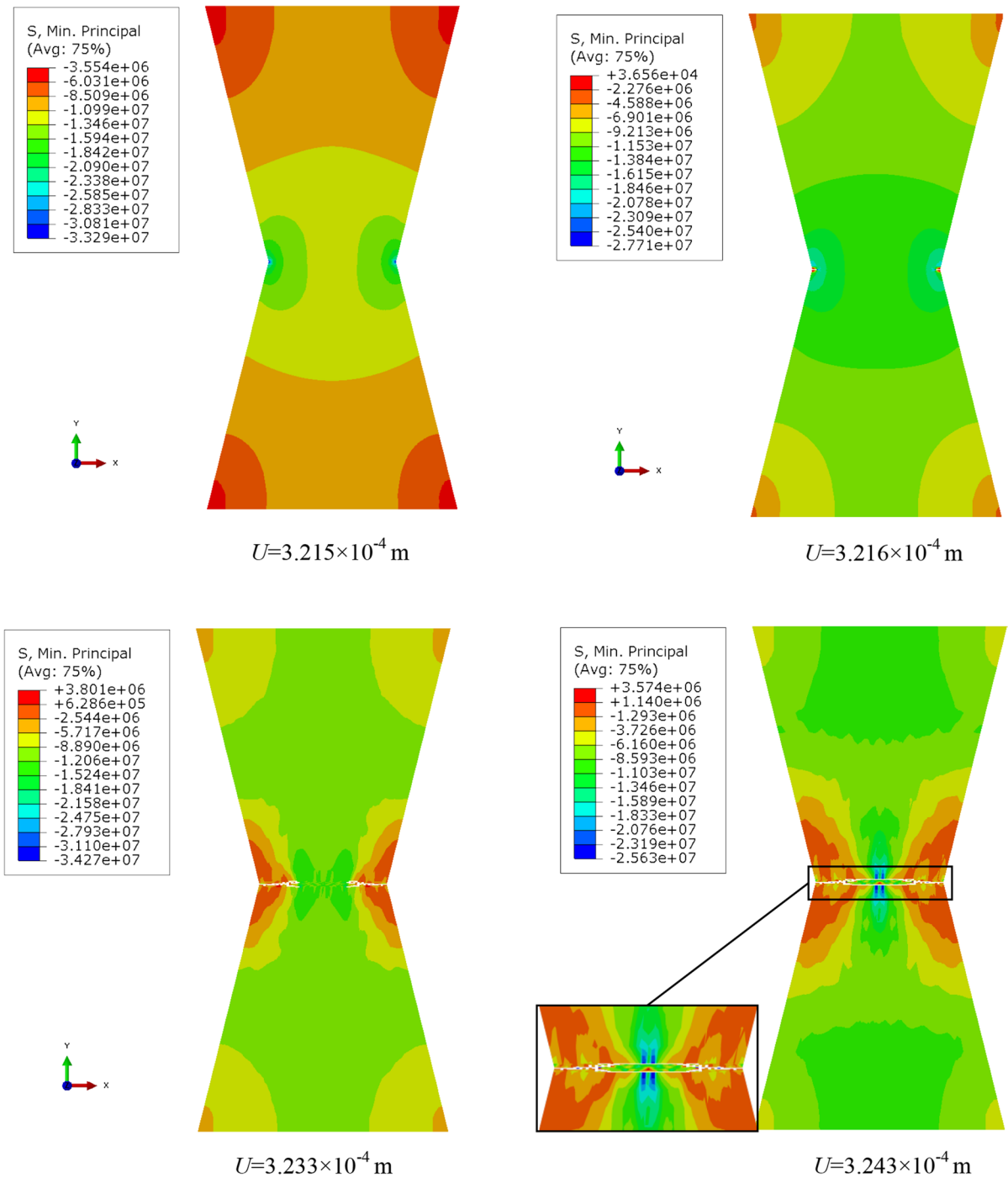


Fig. 4 Dynamic process of model failure under compression (Stress unit unit: Pa)

conditions in Eqs. (1)–(3), the element is identified as broken and deleted, that is, it exits from the iterative calculation of the next load step. The calculation

is repeated until the calculated residuals of all elements meet the convergence criteria, and the stress and deformation results of the elements are output.

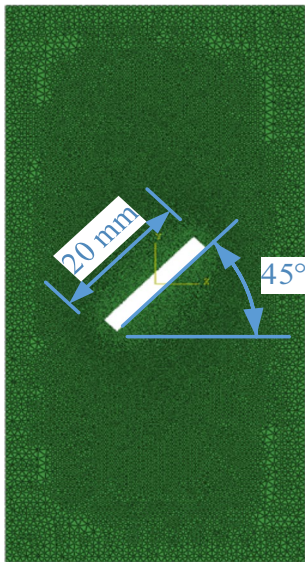


Fig. 5 Calculation model

This section integrates the above three failure criteria into the VUMAT subroutine to simulate the uniaxial compression test process of rock specimens with prefabricated holes. The advantage of this system is that it can better simulate the crack propagation of rock under various failures under complex stress. The numerical simulation process is shown in Fig. 7.

Numerical model size: $H \times W \times T = 120 \text{ mm} \times 60 \text{ mm} \times 30 \text{ mm}$. In the model, a 10 mm diameter hole was prefabricated, and a 12 mm length crack was prefabricated on both sides of the hole, with a width of 2.5 mm and a dip angle of 45° . The elastic modulus of the material is 8.69 GPa, the average compressive strength is 19.32 MPa, the ratio of compression strength to tensile strength is 10, Poisson's ratio is 0.33, and the density is $2600 \text{ kg} \cdot \text{m}^{-3}$ (Cheng et al. 2012) (Fig. 8).

Figure 9 shows the process of simulated crack propagation. In the process of loading, the stress concentration near the microcrack tip results in a small range of crushing and self-similar failure. Then the cracking occurs in the tensile stress concentration area. The precast microcrack tip generates crevices and expands vertically along the precast crack ($U = 8.404 \times 10^{-6} \text{ m}$). Then the crack changes direction and bends in the main direction of axial compression ($U = 1.009 \times 10^{-5} \text{ m}$). With the increase of axial stress, the upper and lower ends of the crack generate

reverse wing crack ($U = 1.800 \times 10^{-5} \text{ m}$), and the secondary tensile crack develops along the horizontal direction to form tensile failure ($U = 4.427 \times 10^{-5} \text{ m}$). Finally, the specimen is destroyed completely. The simulation results of the model are basically consistent with the simulation results of Guo (2020) using the RFP system (Fig. 10). It shows that the simulation system of fracture propagation proposed in this paper is reasonable and correct.

3 Results and Analysis

Section 2.4 shows the failure characteristics of specimens. This section analyzes the causes of crack growth in detail. In order to obtain the stress distribution information around the fracture, in the VUMAT subroutine, the calculation results of M–C and the calculation results of maximum principal stress and minimum principal stress at each integral step state are respectively assigned to the state variable, which appear in the form of SDV in the Visualization plate of ABAQUS software. SDV2, SDV3 and SDV4 respectively represent the values of M–C criterion, maximum principal stress and minimum principal stress in each integral state.

Figure 11a shows the distribution of maximum principal stress around cracks at each analysis step. Most areas on both sides of the opening crack are strained. The tensile zone of the lower part of the fracture is obviously larger than that of the upper part (Wang 2009). The maximum tensile stress concentration area is near the crack tip. With the increase of axial stress, the prefabricated crack expands and the tensile stress distribution inside the specimen changes. The wing crack propagates in the tensile stress concentration area and its position varies with the crack tip during the anti-wing crack propagation.

Figure 11b reveals the distribution of the minimum principal stress around the crack at each analysis step. The maximum compressive stress is concentrated near the crack tip. With the load increases, the maximum compressive stress value increases and the concentration phenomenon becomes more obvious.

Figure 11c shows the distribution of shear stress around the crack at each analysis step. The area of maximum compressive-shear stress is close to the inside of the crack, and the area of maximum tensile-shear stress is at the tip of the crack. With

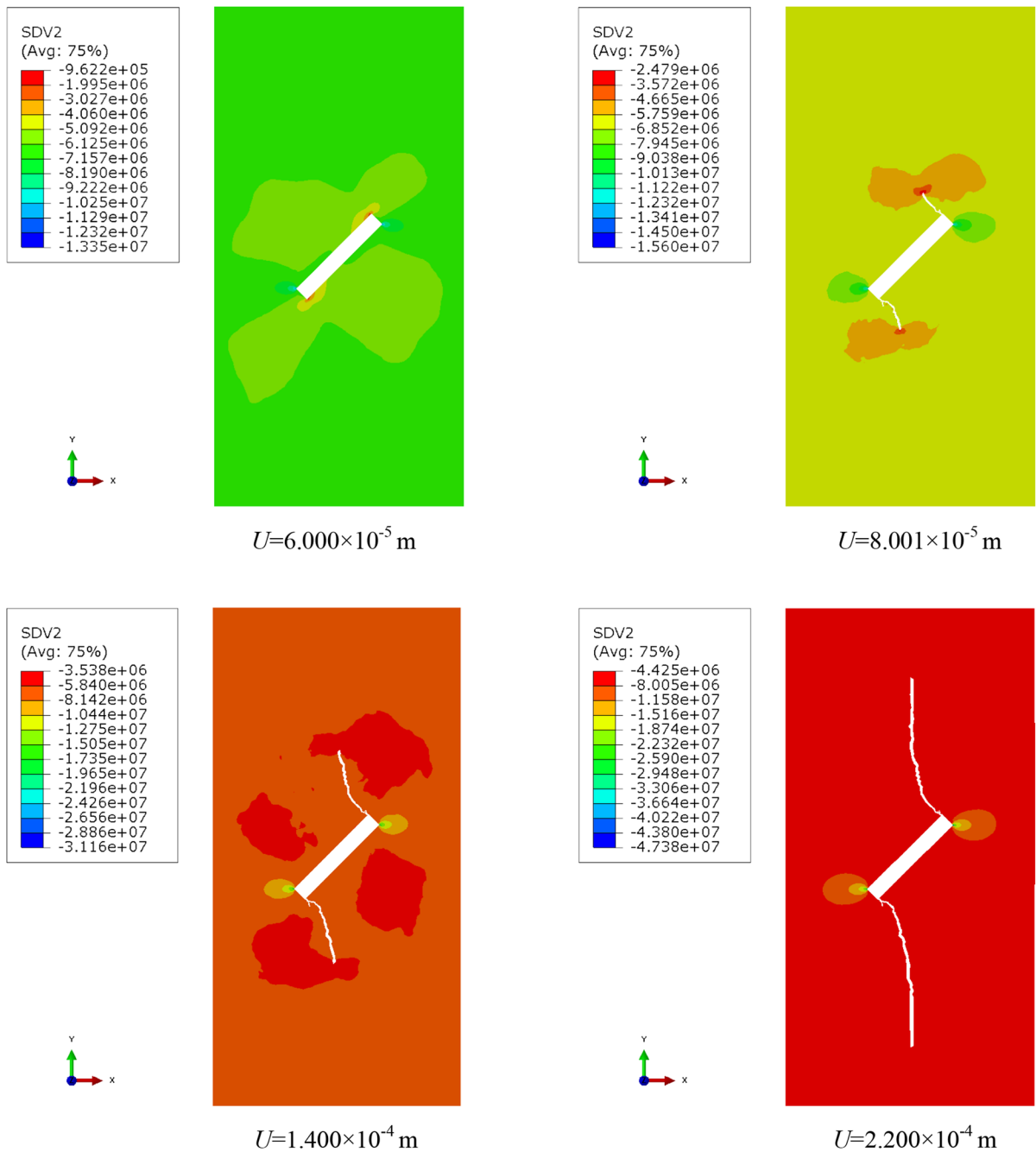


Fig. 6 Dynamic failure process of the model based on M–C criterion [Stress unit: Pa, SDV2 represents the calculated value of formula (2–3)]

the increase of the load, the maximum compressive-shear stress area and the maximum tensile-shear stress area continue to move horizontally along the crack tip.

In the early loading stage, the maximum shear stress area and the minimum principal stress maximum area were mainly concentrated in the horizontal crack tip area of the prefabricated crack, while the

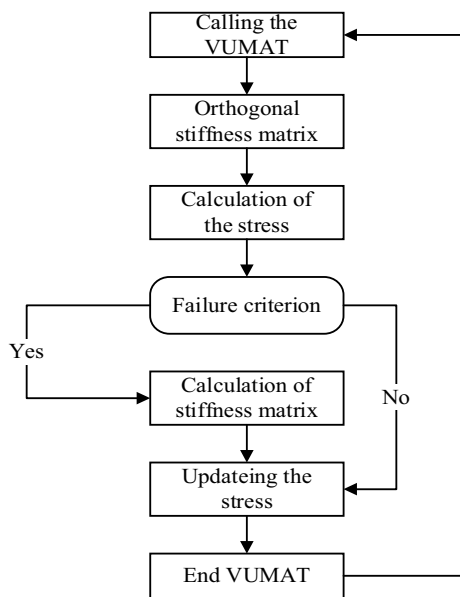


Fig. 7 Numerical simulation flow chart

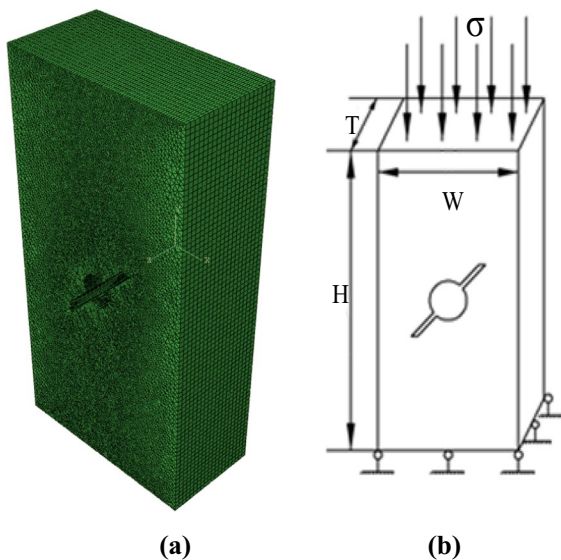


Fig. 8 The calculation model of the verification example

maximum principal stress area was mainly concentrated in the vertical crack tip area. With the increase of the load, the vertical stress state of the crack tip

conforms to the maximum principal stress failure criterion and the failure occurs first. After a while the stress state in the horizontal direction of the crack tip was in accordance with M–C failure criterion. In the whole process, the crack propagation direction in the compressive shear stress field is along the direction of the maximum tensile stress. The minimum principal stress failure criterion has little contribution to failure under compression.

4 Conclusions

According to the above analysis, the following conclusions can be obtained:

1. Wing crack and anti-wing crack are caused by failure criterion of maximum principal stress. The wing crack propagation occurred earlier and the reverse wing crack propagation occurred later.
2. The horizontal shear failure of the precast crack tip is caused by M–C failure criterion, and the crack propagation occurs later than the wing crack and earlier than the anti-wing crack.
3. In the whole compression failure process, the minimum principal stress failure criterion has little contribution to the failure.
4. The reliability of the simulation system is proved by comparing the simulation results with the verification examples and test results.
5. Compared with other rock fracture simulation methods, the advantage of this method is that it combines the maximum compressive stress, maximum tensile stress and M–C failure criterion into VUMAT subroutine, takes it as the failure criterion of matrix element under complex stress, and establishes the simulation program. The failure element deletion algorithm is introduced to investigate the deformation and failure process of rock blocks under load. The model can well simulate the fracture propagation under the mixed mode of compression, tension and shear, rather than only limited to specific cases.

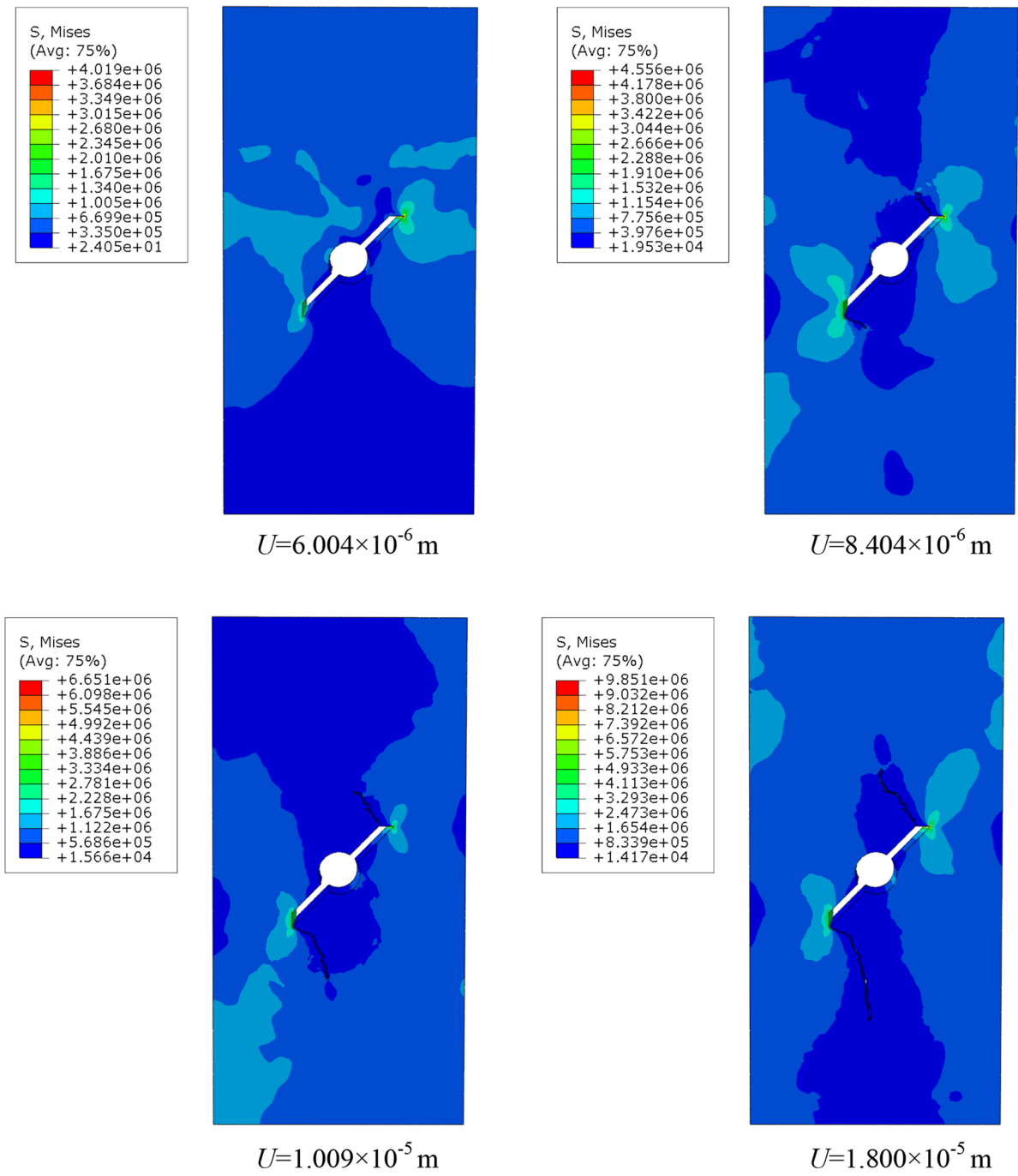


Fig. 9 Results of Real-time crack propagation (Stress unit: Pa)

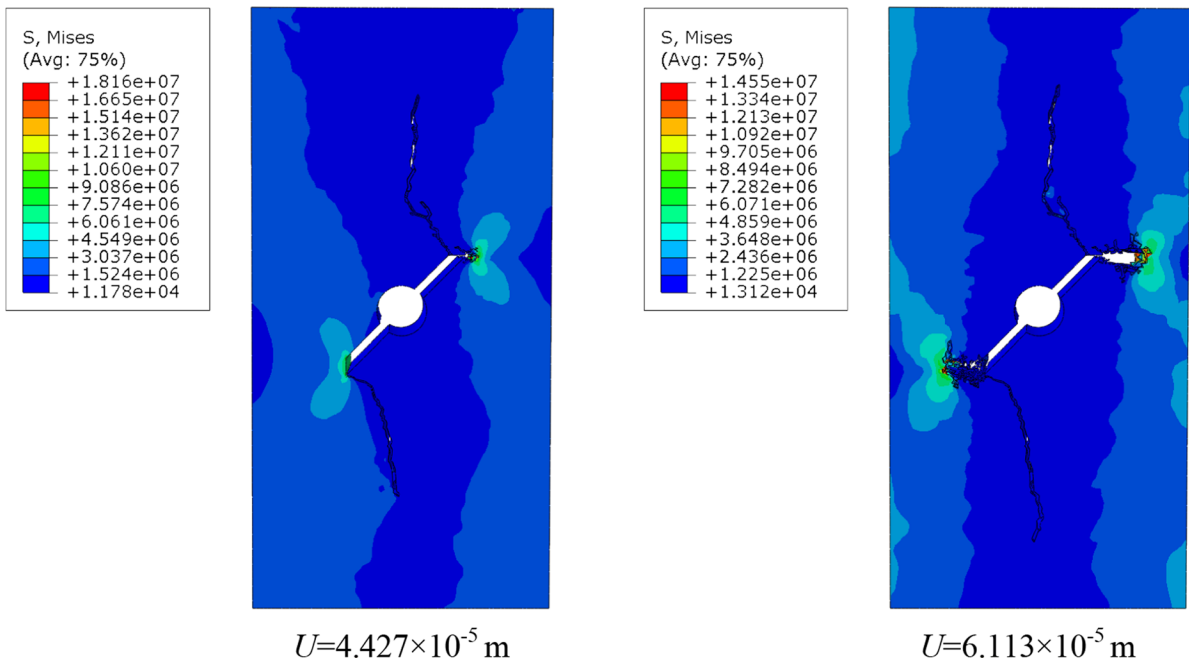
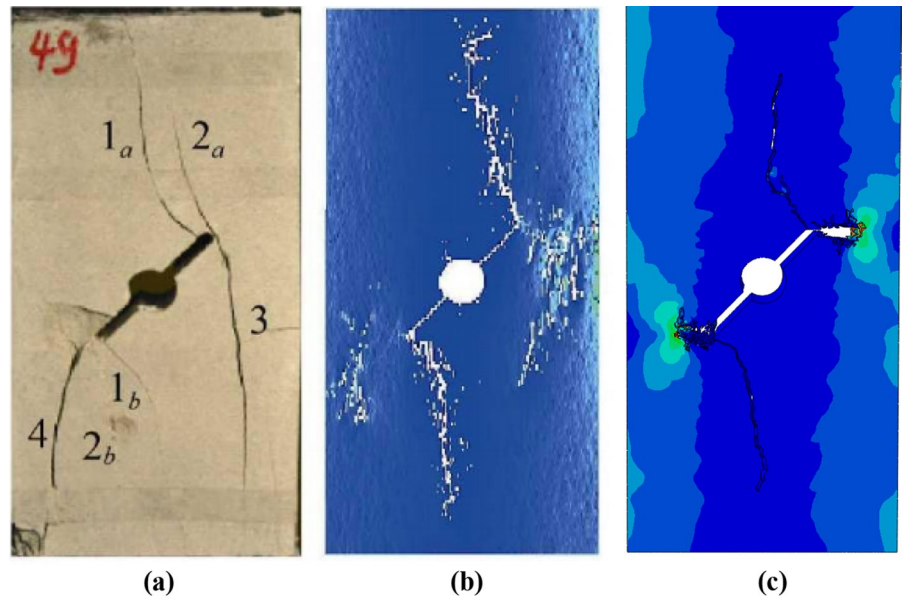
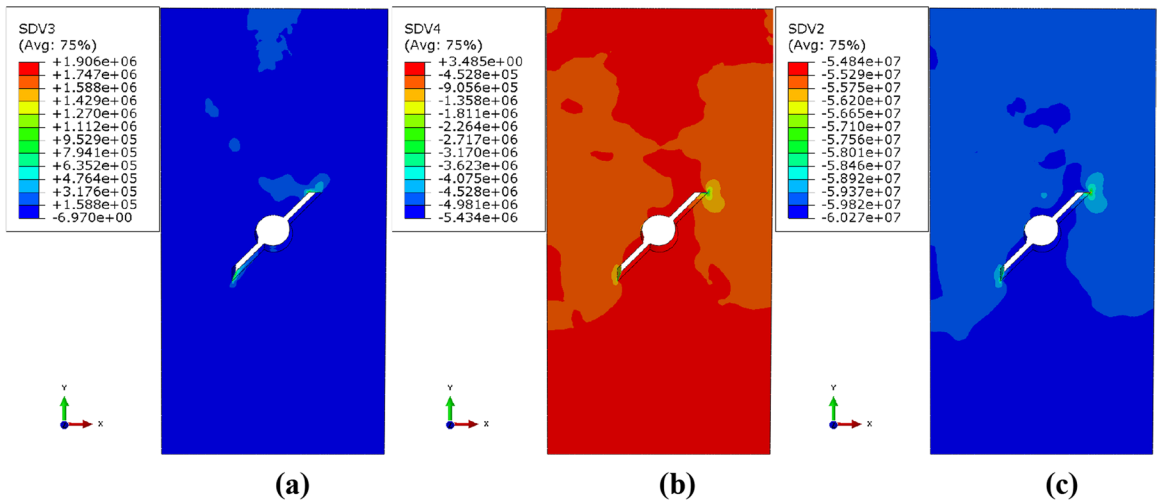


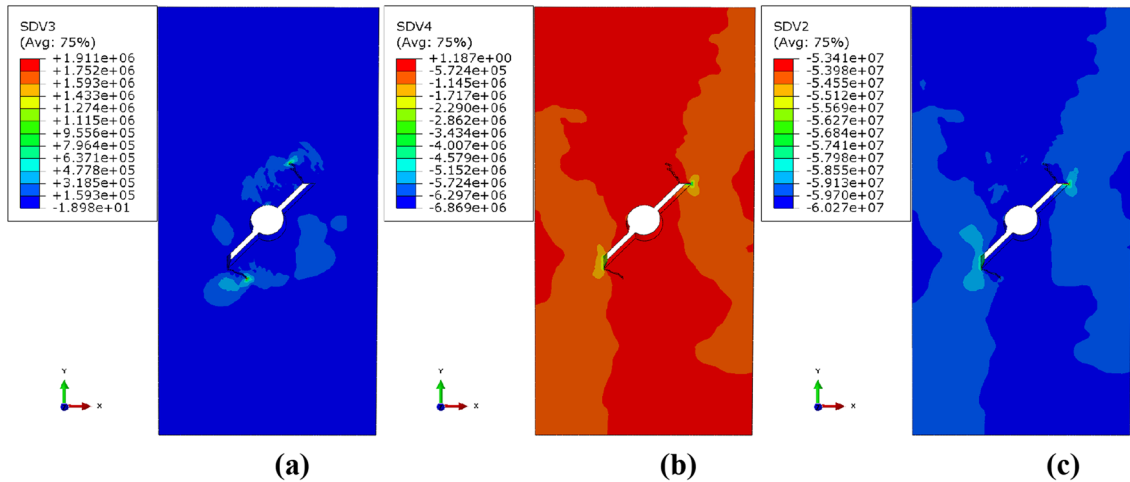
Fig. 9 (continued)

Fig. 10 Comparison of results between numerical simulation and calculation example: **a** is the test result of Cheng et al. (2012); **b** is the simulation result of Guo (2020); **c** is the simulation result of this paper

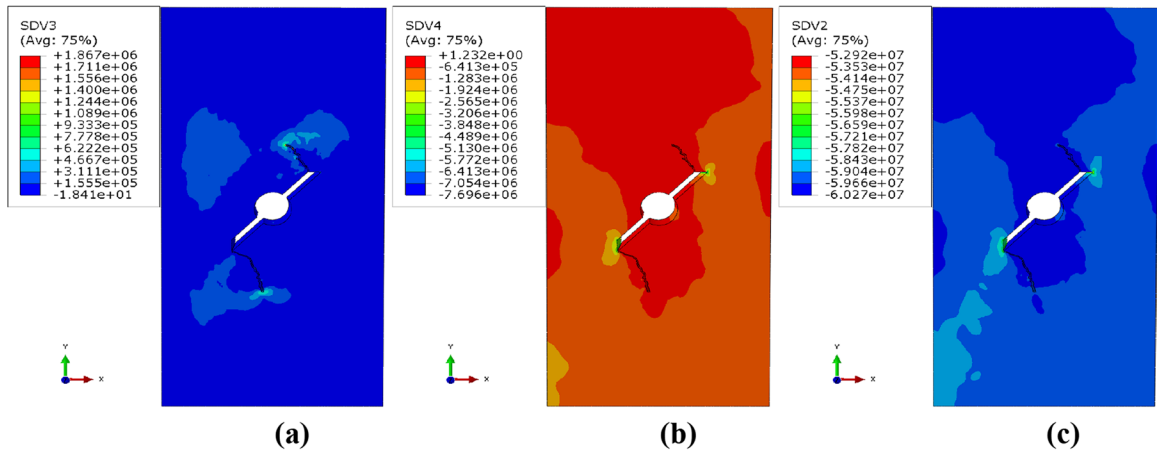




$U=6.004 \times 10^{-6} \text{ m}$

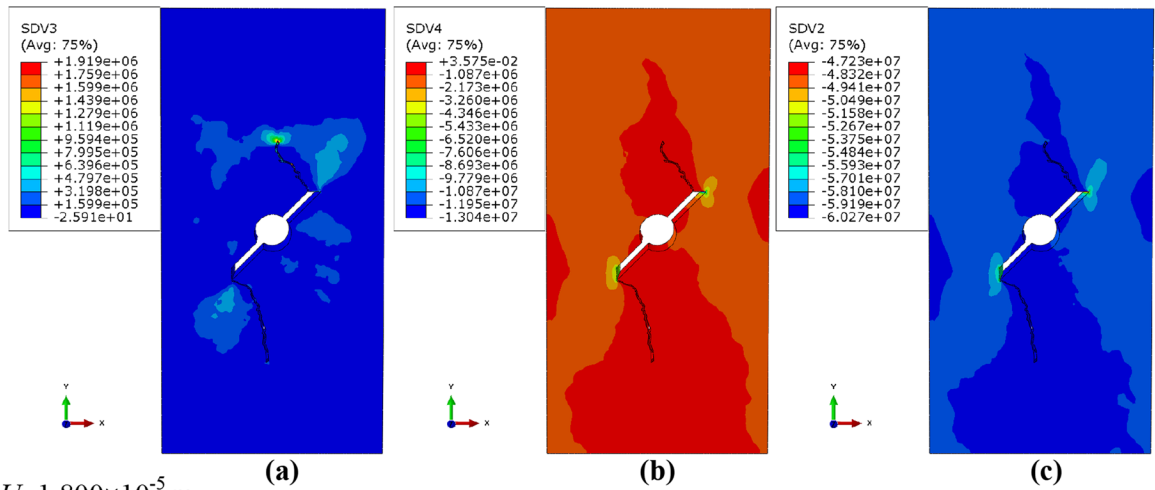


$U=8.404 \times 10^{-6} \text{ m}$

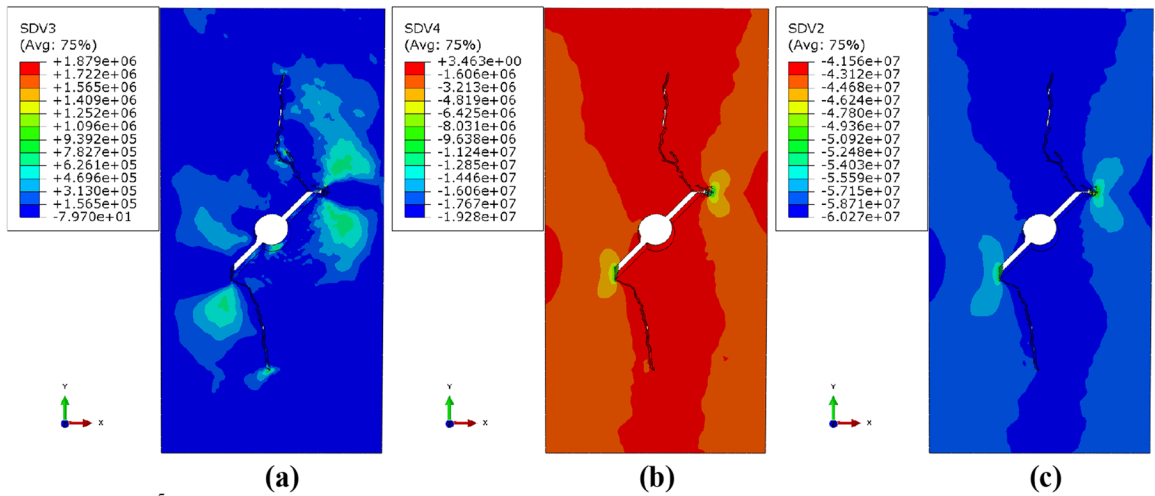


$U=1.009 \times 10^{-5} \text{ m}$

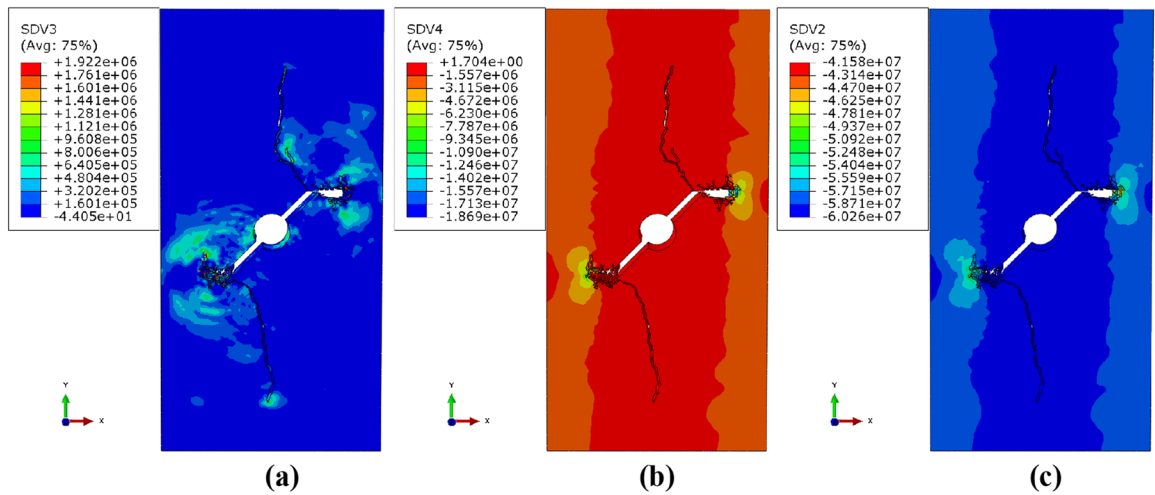
Fig. 11 Comparison of fracture expansion results under different state variables (Stress unit: Pa)



$U=1.800 \times 10^{-5} \text{ m}$



$U=4.427 \times 10^{-5} \text{ m}$



$U=6.113 \times 10^{-5} \text{ m}$

Fig. 11 (continued)

Acknowledgements This work is financially supported by the National Natural Science Foundation of China (No. 51804182), the Plan for Outstanding Youth Innovation Teams in College and University of Shandong Province, China (No. 2019KJG007), the Shandong Provincial Natural Science Foundation, China (No. ZR2020ME097). The Graduate Education Quality Improvement Plan of Shandong Province, China (No. SDYAL21062).

Funding The authors have not disclosed any funding.

Data Availability Enquiries about data availability should be directed to the authors.

Declarations

Conflict of interest The authors declare that they have no known competing financial interests or personal relationships that could have appeared to influence the work reported in this paper.

References

- Aliabadian Z, Sharafisafa M, Mortazavi A, Maarefvand P (2014) Wave and fracture propagation in continuum and faulted rock masses: distinct element modeling. *Arab J Geosci* 7:5021–5035
- Chen JC, Zhou L, Chemenda AI, Xia BW, Su XP, Shen ZH (2020) Numerical modeling of fracture process using a new fracture constitutive model with applications to 2D and 3D engineering cases. *Energy Sci Eng* 8(7):2628–2647
- Cheng L, Yang SQ, Liu XG (2012) Test and simulation study on crack growth characteristics of defective sandstone. *J Min Saf Eng* 29(05):719–724 ((in Chinese))
- Feng Y, Gray K (2019) XFEM-based cohesive zone approach for modeling near-wellbore hydraulic fracture complexity. *Acta Geotech* 14:377–402
- Gui YL, Zhao ZY, Zhou HY, Wu W (2016) Numerical simulation of P-wave propagation in rock mass with granular material-filled fractures using hybrid continuum-discrete element method. *Rock Mech Rock Eng* 49:4049–4060
- Guo XC (2020) Numerical simulation of pore and fracture propagation under uniaxial stress. *Coal Geol Explor* 48(02):179–186+194 ((in Chinese))
- Huang JW, Jin TY, Chai Z, Barrufet M, Killough J (2019) Compositional simulation of fractured shale reservoir with distribution of nanopores using coupled multi-porosity and EDFM method. *J Petrol Sci Eng* 179:1078–1089
- Li K, Wang Y, Huang X (2012) DDM regression analysis of the in-situ stress field in a non-linear fault zone. *Int J Miner Metall Mater* 19:567–573
- Li K, Huang L, Huang X (2014) Propagation simulation and dilatancy analysis of rock joint using displacement discontinuity method. *J Cent South Univ* 21:1184–1189
- Li TC, Lyu LX, Zhang SL, Sun JC (2015) Development and application of a statistical constitutive model of damaged rock affected by the load-bearing capacity of damaged elements. *J Zhejiang Univ Sci A* 16:644–655
- Li TC (2005) CT test and theoretical analysis of three-dimensional fracture propagation. Graduate University of Chinese Academy of Sciences (Wuhan Institute of Rock and Soil Mechanics) Wuhan Hubei China ((in Chinese))
- Li X (2012) Gleeble Numerical simulation and experimental verification of Joule Effect in thermo-mechanical simulation. Shanghai Jiao Tong University Shanghai China ((in Chinese))
- Marji MF (2015) Simulation of crack coalescence mechanism underneath single and double disc cutters by higher order displacement discontinuity method. *J Cent South Univ* 22:1045–1054
- Matsuda Y, Iwase Y (2002) Numerical simulation of rock fracture using three-dimensional extended discrete element method. *Earth Planet Spce* 54:367–378
- Miao ST, Pan PZ, Wu ZH, Li SJ, Zhao SK (2018) Fracture analysis of sandstone with a single filled flaw under uniaxial compression. *Eng Fract Mech* 204:319–334
- Ofoegbu GI, Smart KJ (2019) Modeling discrete fractures in continuum analysis and insights for fracture propagation and mechanical behavior of fractured rock. *Rineng* 4:100070
- Qian XK, Liang ZZ, Liao ZY, Wang K (2020) Numerical investigation of dynamic fracture in rock specimens containing a pre-existing surface flaw with different dip angles. *Eng Fract Mech* 223:106675
- Sanchez ECM, Cordero JAR, Roehl D (2020) Numerical simulation of three-dimensional fracture interaction. *Comput Geotech* 122:10352
- Sheng M, Li GS, Sutula D, Tian SC, Stephane PAB (2018) XFEM modeling of multistage hydraulic fracturing in anisotropic shale formations. *J Petrol Sci Eng* 162:801–812
- Silva VRSD, Ranjith PG (2020) A study of rock joint influence on rock fracturing using a static fracture stimulation method. *J Mech Phys Solids* 137:103817
- Sun HF, Yang YM, Ju Y, Zhang QG, Peng RD (2014) Numerical analysis of coal and rock deformation failure and energy release under excavation unloading condition. *J China Coal Soc* 39(02):258–272 ((in Chinese))
- Sun H, Liu XL, Zhang SG, Nawit K (2020) Experimental investigation of acoustic emission and infrared radiation thermography of dynamic fracturing process of hard-rock pillar in extremely steep and thick coal seams. *Eng Fract Mech* 226:06845
- Tang JH, Chen XD, Dai F (2020) Experimental study on the crack propagation and acoustic emission characteristics of notched rock beams under post-peak cyclic loading. *Eng Fract Mech* 226:106890
- Tang Q, Li YA (2015) Particle flow simulation of the effect of confining pressure on rock crack propagation. *J Changjiang Acad Sci* 32(04):81–85 ((in Chinese))
- Tripoppoom S, Yu W, Huang HY, Sepehrnoori K, Song WJ, Dachuwanattana S (2019) A practical and efficient iterative history matching workflow for shale gas well coupling multiple objective functions, multiple proxy-based MCMC and EDFM. *J Petrol Sci Eng* 176:594–611 ((in Chinese))
- Trivino LF, Mohanty B (2015) Assessment of crack initiation and propagation in rock from explosion-induced stress

- waves and gas expansion by cross-hole seismometry and FEM-DEM method. *Int J Rock Mech Min* 77:287–299
- Wang H, Jiang C, Zheng PQ, Zhao WJ, Li N (2020b) A combined supporting system based on filled-wall method for semi coal-rock roadways with large deformations. *Tunn Undergr Sp Tech* 99:103382. <https://doi.org/10.1016/j.tust.2020.103382>
- Wang T, Liu ZL, Zeng QL, Gao Ym, Zhong Z (2017) XFEM modeling of hydraulic fracture in porous rocks with natural fractures. *Sci China Phys Mech* 60:084612
- Wang C, Ran QQ, Wu YS (2019) Robust implementations of the 3D-EDFM algorithm for reservoir simulation with complicated hydraulic fractures. *J Petrol Sci Eng* 81:106229
- Wang S, Li DG, Mitri H, Li HM (2020a) Numerical simulation of hydraulic fracture deflection influenced by slotted directional boreholes using XFEM with a modified rock fracture energy model. *J Petrol Sci Eng* 193:107375
- Wang H, Jiang C, Zheng PQ, Li N, Zhan YB (2020c) Deformation and failure mechanism of surrounding rocks in crossed-roadway and its support strategy. *Eng Fail Anal* 116:104743. <https://doi.org/10.1016/j.engfailanal.2020c.104743>
- Wang H (2009) Research on fracture propagation mechanism and Numerical Simulation on three-dimensional surface of rock. Shandong University of Science and Technology Qingdao Shandong China (in Chinese)
- Wu ZJ, Zhang PL, Fan LF, Liu QS (2019) Numerical study of the effect of confining pressure on the rock breakage efficiency and fragment size distribution of a TBM cutter using a coupled FEM-DEM method. *Tunn Undergr Sp Tech* 88:260–275
- Wu GS, Yu WJ, Zuo JP, Du SH (2020a) Experimental and theoretical investigation on mechanisms performance of the rock-coal-bolt (RCB) composite system. *Int J Min Sci Technol* 30(6):759–768
- Wu Z, Zhou Y, Weng, L, Liu QS, Xiao Y (2020b) Investigation of thermal-induced damage in fractured rock mass by coupled FEM-DEM method. *Comput Geosci*
- Xia ZG, Wang KY, Ge FY (2020) Special hole elements for simulating the heat conduction in two-dimensional cellular materials. *Compos Struct* 246:112383
- Yang WM, Geng Y, Zhou ZQ, Li LP, Gao CL, Wang MX, Zhang DS (2020) DEM numerical simulation study on fracture propagation of synchronous fracturing in a double fracture rock mass. *Geomech Geophys Geo-Energ Geo-Resour* 6:39
- Yu WJ, Wu GS, Pan B, Wu QH, Liao Z (2021) Experimental investigation of the mechanical properties of sandstone-coal-bolt specimens with different angles under conventional triaxial compression. *Int J Geomech* 21(6):04021067

Publisher's Note Springer Nature remains neutral with regard to jurisdictional claims in published maps and institutional affiliations.